Received: 27 January 2023 | Revised: 13 March 2023 | Accepted: 13 March 2023

DOI: 10.1002/bio.4487

RESEARCH ARTICLE

LUMINESCENCE The Journal of Biological and Chemical Luminescence WILEY

Preparation of novel authentication film by screen printing of anthocyanin biomolecular extract: Thermochromism and vapochromism

Afrah M. Aldawsari[1,2] | Nada D. Alkhathami[3] | Ameena M. Al-bonayan[1] | Hussain Alessa[1] | Kholood M. Alkhamis[3] | Hana M. Abumelha[4] | Nashwa M. El-Metwaly[1,5]

[1]Department of Chemistry, Faculty of Applied Sciences, Umm Al-Qura University, Makkah, Saudi Arabia

[2]King Abdulaziz City for Science and Technology, Riyadh, Saudi Arabia

[3]Department of Chemistry, College of Science, University of Tabuk, Tabuk, Saudi Arabia

[4]Department of Chemistry, College of Science, Princess Nourah bint Abdulrahman University, Riyadh, Saudi Arabia

[5]Department of Chemistry, Faculty of Science, Mansoura University, Mansoura, Egypt

Correspondence
Nashwa El-Metwaly, Department of Chemistry, Faculty of Applied Sciences, Umm Al-Qura University, Makkah, Saudi Arabia.
Email: n_elmetwaly00@yahoo.com; nmmohamed@uqu.edu.sa

Funding information
Princess Nourah bint Abdulrahman University Researchers Supporting, Grant/Award Number: PNURSP2023R22

Abstract

Novel thermochromic and vapochromic paper substrates were prepared via screen printing with anthocyanin extract in the presence of ferrous sulfate mordant, resulting in multi-stimuli responsive colorimetric paper sheets. Environmentally friendly anthocyanin extract was obtained from red-cabbage (*Brassica oleracea* var. *capitata* L.) to function as spectroscopic probe in coordination with ferrous sulfate mordant. Pink anthocyanin/resin nanocomposite films immobilized onto paper surface were developed by well-dispersion of anthocyanin extract as a colorimetric probe in a binding agent without agglomeration. As demonstrated by CIE colorimetric studies, the pink ($\lambda_{max} = 418$ nm) film deposited onto paper surface turns greenish-yellow ($\lambda_{max} = 552$ nm) upon heating from 25 to 75°C, demonstrating new thermochromic film for anti-counterfeiting applications. The thermochromic effects were investigated at different concentrations of the anthocyanin extract. Upon exposure to ammonia gas, the color of the anthocyanin-printed sheets changes rapidly from pink to greenish-yellow, and then immediately returns to pink after taking the gaseous ammonia stimulus away, demonstrating vapochromic effect. The current sensor strip showed a detection limit for ammonia gas in the range 50–300 ppm. Both thermochromism and vapochromism showed high reversibility without fatigue. In addition to studying the rheological properties of the prepared composites, the morphological and mechanical properties of the printed cellulose substrates were also studied.

KEYWORDS
ammonia sensor, *Brassica oleracea* var. *capitata* L, screen printing, smart ink, thermochromic

1 | INTRODUCTION

Identification papers, travel documents, driver's licenses, currency, legal documents, birth and death certificates, and court records are all examples of documents that have been used to secure sensitive information [1–3]. Paper documents are very valuable and must be protected against forgery. Counterfeiting is the practice of making fake versions of legitimate goods and services [4]. Document falsification also includes the practice of adding, erasing, or eradicating text from a document. Therefore, it is essential to check the legitimacy of documents. Annually, counterfeiting causes a loss of billions of dollars. Additionally, human health and safety could be at risk if medical products were made using counterfeited parts. This has increased the need for innovative, cost-effective, and efficient anti-counterfeiting

strategies [5]. Numerous indicator materials, including polymer nanoparticles, DNA, metal-based emulsions, and peptides have been employed to verify the genuineness of products [6–8]. There are three examination stages of verification that must be considered before a document can be described genuine. The first step in the examination procedure involves visual identification, and it occurs when a person determines whether or not a document has characteristics like watermarks or holograms. The second phase of examination employs an ultraviolet supply, a barcode scanning tool, and photoluminescent pigments. In the third phase of examination, specialized forensic laboratory equipment, including electron microscopic devices and spectrophotometers are utilized to investigate the finer details of the document [9–11]. Documents can be protected by embedding an indicator material in a printed artwork that is then stapled onto paper sheets. To prevent sensitive information from being erased by chemicals or solvents like bleaching agents, it is possible to include chemical indicators into the paper-making process as markers. It has been suggested that bleaching might oxidize chemical markers to leave behind lasting signs that signal a trial of counterfeiting has taken place [12, 13]. The solvent indicator can be inserted onto the document surface to detect any dyestuff leakage. Counterfeiting can be thwarted by printing different patterns with chemical markers on the paper surface. Using the three-dimensional printing capability of intaglio as a concealed image, some protective patterns can expose the validity of papers when seen from acute angles. Modulations of screen angles and the dot frequencies are two examples of digital scan traps employed in today's pattern creation processes [14]. Another type of document protection is optical image encoding, which safeguards a series of images that appear progressively when the paper document is slanted. However, most of the photochromic and fluorescent methods are costly and complicated. Additionally, the use of ultraviolet light for the detection of photochromic effects has been very dangerous due to the serious health issues that can be caused by ultraviolet light, such as skin cancer, genetic defects, immune system suppression and potentially blinding eye diseases [15–17]. However, colorimetric thermochromism has been reported as a simple, cheap, and efficient approach for the development of anti-counterfeiting documents. The colorimetric thermochromic materials have the ability to change color when influenced by heat. A simple method of authentication is the use of thermochromic designs to be monitored by increasing temperature. Protecting contents on the surface of documents with thermochromic materials is a simple, efficient and reliable authentication method [18]. The thermochromic compounds can be used as security agents to prevent the manipulation of vital information since they are destroyed when peeled off or scraped. The functionalization of anti-counterfeiting document manufacture relies on the use of optical patterns on the documents themselves, which are simple to read and difficult to duplicate [19]. A material thermochromism indicates its capacity to alter its hue in response to exposure to temperature increase. Some applications of thermochromic materials include anti-counterfeiting composites for use in creating security barcodes [20]. The exposure to a heat source causes a reversible color shift in this security authentication barcode. The development of thermochromic smart devices has been reported for various applications, such as eyeglasses, smart window, and sensors [21, 22].

Several synthetic spectroscopic probes, such as tricyanofuran-hydrazone and boron-dipyrromethene, have been reported as thermochromic chemicals. However, these synthetic spectroscopic probes are neither biodegradable nor biocompatible. Synthetic spectroscopic probes are usually harmful to both environment and human health [23, 24]. Anthocyanins are water-soluble dyestuffs that, relying on the pH of the surrounding medium, appear in various colors, including black, blue, purple, green, red and colorless. Food plants are rich in anthocyanins, such as raspberry, blueberry, red-cabbage and black soybean. Anthocyanins can be classified as flavonoids that are generated using the phenylpropanoid procedure [25–27]. They exist in all tissues of higher plants, including fruits, flowers, roots, stems, and leaves. Anthocyanins are derived from the anthocyanidin structure by the inclusion of sugars. Anthocyanins have been used as safe color additives for foodstuffs, which have been approved by the European Union. Thus, anthocyanins have no impact on human biology or diseases [28]. However, they have been reported as antioxidant and anticancer agents owing to their capability to quench active oxygen species. Anthocyanins have been used as colorimetric pH indicators due to their ability to change color with changing the pH of the surrounding medium [29]. They provide red color in very low acid solutions, pink in low acid solutions, purple in neutral media, greenish-yellow in low basic media, and colorless in very high basic media. Research on anthocyanins has been extensively explored because of their potential use in the creation of multi-stimuli responsive materials [30, 31]. Because of their capacity to change color upon application of heat, anthocyanins have found utility in thermochromic devices. Additionally, anthocyanins have been reported as efficient vapochromic and biochromic colorimetric agents for the detection of various toxic agents, such as ammonia and urea [25, 26]. In comparison to other organic molecular probes, anthocyanins are highly reversible, biodegradable, biocompatible, inexpensive, and stable. Thus, it is suggested that anthocyanin-based spectroscopic active sites are a great option for delivering thermochromic anti-counterfeiting to paper documents without affecting the paper key attributes, including mechanical behavior and appearance [32, 33].

Herein, we present the screen printing of anthocyanin-based spectroscopic active sites to create thermochromic, and vapochromic, paper sheets. The printed film was pink under ambient conditions but became greenish-yellow upon increasing temperature or exposure to toxic ammonia. Therefore, anthocyanin-printed document can be used without fear of a counterfeit version being substituted, scratched, or erased. The anthocyanin sensor was isolated from red-cabbage by a simple procedure in an acidic aqueous solution [33]. There are polar functional hydroxyl groups and various molecular switching forms, including chalcone, flavylium, quinonoidal and carbinol, in the produced anthocyanin probe [31]. This makes it an excellent candidate for incorporation into various ink formulations. In order to produce thermochromic anti-counterfeiting prints onto paper documents, a combination of binding agent and an anthocyanin probe was applied. Anthocyanins can be described as direct dyes, which are highly water-

soluble [26]. Therefore, the deposition of anthocyanins into paper surface can be efficiently carried out using ferrous sulfate mordant. Both anthocyanin biomolecules and paper-based cellulose biological macromolecule are excellent choices as they are environmentally friendly and non-toxic natural products. The printing process was made in the presence of ferrous sulfate to fasten the water-soluble anthocyanins onto the paper surface. Heat fixation was used to form a three-dimensional coating of crosslinked resin binder onto the paper surface, entrapping the anthocyanin probe. The colorimetric variations of the printed film were analyzed by absorption spectra and CIELab parameters, and the findings confirmed an efficient authentication of the thermochromic film. The vapochromism, thermochromism and surface morphology were investigated using a range of analytical approaches. The chemical structure of the extracted anthocyanin was analyzed by high-performance liquid chromatography (HPLC). Nanoparticle production in an aqueous dispersion of a mordant–anthocyanin complex was confirmed by transmission electron microscopy (TEM) to indicate diameters of 4–19 nm. The rheological, mechanical, and photostability studies were also conducted. Due to its promising colorimetric features, anti-counterfeiting stamps can be developed using the current anthocyanin-based thermochromic nanocomposite.

2 | EXPERIMENTAL

2.1 | Materials

Hydrochloric acid (HCl; ACS Reagent; 37%) and ferrous sulfate were obtained from Aldrich (Egypt). The resin acid binding agent was supplied from Dystar (Egypt). The acetylene diol, mineral oil, and oleoresin were purchased from Merck (Egypt). In order to print the thermochromic patterns, off-white Whatman sheets were supplied from Sigma-Aldrich (Egypt) with diameter of 240 mm, weight of 87 g/m^2, and a pore size of 11 µm, and thickness of 180 µm. The red-cabbage was obtained from the local market (Egypt).

2.2 | Preparation of anthocyanidin extract

According to previous procedures [33], *Brassica oleracea* L. var. *capitata* (600 g) was exposed to crushing and maceration in a 300 mL mixture of methanol and distilled water (3:1). Aqueous HCl (1 mol/L) was poured into the solution to decrease the pH value to 2. The mixture was stored in a fridge at 4°C for 3 days. The combination was then filtered, and centrifuged (2200 rpm) for 10 min. The solid residues were removed, and the remaining red solution was subjected to an extraction process using chloroform. The chloroform was then evaporated by rotary-evaporator at 45°C. The obtained solution was refluxed with concentrated HCl in a water bath to yield a reddish-violet color. The provided solution was chilled till a deep brown powder (anthocyanidin chloride) precipitated. The mixture was filtered under vacuum, and dried in a desiccator. Methyl alcohol was utilized as eluent in the Sephadex LH-20 refinement method. In order to explore its chemical composition, the provided anthocyanidin solid powder was dissolved (1.5 mg) in methanol (5 mL) to afford a standard solution that was cooled in a fridge for an hour to reach equilibrium. The anthocyanidin extract methanolic solution was studied by HPLC Agilent 1100 (Waldborn, Germany). The flavonoid nature of anthocyanidin was tested by Shinoda experiment [25], whereby a tiny piece of magnesium ribbon and HCl (1 mL) were added to the standard methanolic solution of anthocyanidin to generate a red color.

2.3 | Preparation of thermochromic documents

A mixture of ammonium hydroxide (NH_4OH, 1% w/w), oleoresin (55% w/w), mineral oil (10% w/w), alkyd resin (20% w/w), dryer (0.5% w/w), and anthocyanin probe were stirred for 2 h to achieve a homogeneous distribution. The alkyd resin was employed to enhance the print transferring process and the print gloss appearance. The dryer was applied to fasten the print drying, whereas NH_4OH was employed to amend the pH of the printing composite. Several printing pastes were developed utilizing various ratios of the anthocyanin probe, including 0 (blank; INK_0), 0.1% (INK_1), 0.25% (INK_2), 0.5% (INK_3), 0.75% (INK_4), 1% (INK_5), 1.5% (INK_6), 1.75% (INK_7), and 2% (INK_8) (w/v). Ferrous sulfate mordant (5%) was then added to the prepared mixtures to develop mordant–anthocyanin complex nanoparticles. The mixtures were exposed to homogenization (35 kHz) for 15 min to accomplish a homogeneous distribution. Acetylene diol dispersing agent (1% w/w) was added to the prepared mixtures with stirring to afford a yellowish milky suspension. The produced inks were screen-printed onto paper substrates using a stencil design on a flat silkscreen surface. The printed paper substrates were then air-dried.

2.4 | Methods

The morphologies of prints were analyzed using scanning electron microscopy (SEM) (VEGA3; TESCAN Co. Ltd, Brno, Czech Republic) coupled with TEAM-EDX. TEM (JEOL-1230; JEOL, Tokyo, Japan) was used to measure the particle sizes of the synthesized mordant–anthocyanin complex nanoparticles. The functional groups on the paper surface were analyzed using Fourier-transform infrared (FTIR) spectroscopy (Nicolet Nexus 670). Zwick-Universal testing system (Zwick, Ulm, Germany) was used to measure the mechanical properties of the printed papers. The rheology was studied, and viscosity was calculated at different shear rates using a Brookfield DVIII Rheometer.

2.5 | Thermochromic measurements

The thermochromic behavior of the printed sheets was explored by changing the temperature between 25 and 75°C using a heat gun, and reporting the absorption spectra. The temperature was forced back

and forth in the range 25–75°C to examine the reversibility of thermochromism. The absorbance spectra were measured after every heating/cooling cycle.

2.6 | Colorimetric properties

The printed sheets were subjected to thermochromic and vapochromic studies by analyzing their color strength (*K*/*S*) and CIELab coordinates utilizing an UltraScanPro spectrophotometer (HunterLab, Reston, VA, USA). We examined the print reversibility by taking absorption spectra both before and after several cycles of exposure to heat and ammonia gas. Photographs of printed paper (INK_6) were obtained with a Canon A710IS under vapochromic and thermochromic conditions.

3 | RESULT AND DISCUSSION

3.1 | Morphological features

Anthocyanins can be defined as water-soluble direct dyes. Thus, ferrous sulfate mordant was applied to fix the anthocyanidin spectroscopic probe into the paper surface. The mordant–anthocyanidin nanoparticles were produced by the direct addition of ferrous sulfate into an aqueous solution of anthocyanidin in distilled water. Figure 1 shows that the average diameter of the produced mordant–anthocyanin complex nanoparticles lies between 4 and 19 nm, as measured by TEM. The homogeneous distribution of the mordant–anthocyanin complex particles over the document surface can be attributed to their nano-scale size. According to previous procedure [33], both HCl and methanol were used to extract the anthocyanidin chromophore from *Brassica oleracea* L. var. *capitata* (red-cabbage). The flavonoid and phenolic nature of anthocyanidin were verified by the Shinoda test. The term "smart products" is used to describe materials that can alter one or more of their physical characteristics, such as color, responding to external stimuli. Thermochromic materials, for instance, can alter their appearance in response to heat [20, 21]. Thermochromic anti-counterfeiting paper documents have lately attracted more interest because of their potential usage in several sectors, such as sensors and security alerts.

The Shinoda test [25] was also employed to verify the anthocyanin flavonoid nature, displaying a red color. HPLC analysis was applied to evaluate the anthocyanin extract, indicating the presence of bioactive phenols as summarized in Table 1. The maximum absorption wavelength of a printed paper sheet changed from 418 nm (pink) to 552 nm (greenish-yellow) with rising the temperature from 25 to 75°C, respectively. Anthocyanidin undergoes deprotonation with raising the temperature to result in molecular switching associated with delocalization of electrons. This protonation–deprotonation process is highly reversible under cooling–heating conditions. Four isomeric forms of anthocyanidin were detected upon heating, including quinoid anion, carbinol anion, chalcone, and flavylium cation [31, 32]. At high temperatures, the flavylium positive ion (red) is the dominant isomeric form.

TABLE 1 Phenolic contents of red-cabbage extract as reported by high-performance liquid chromatography (HPLC).

Phenol content	Quantity (wt%)
Catechin	0.75
Chlorogenic acid	2.24
Rutin	20.76
Chrysin	0.82
Acacetin	0.76
Quercetin-7,3′-dimethylether	5.05
Vanillin	0.96
Caffeic acid	0.97
Kaempferol	47.17
Ferulic acid	15.15
Quercetin	3.23
Gallic acid	0.81
Quercetin-7-methylether	0.85
Cinnamic acid	1.48
p-Coumaric acid	2.49

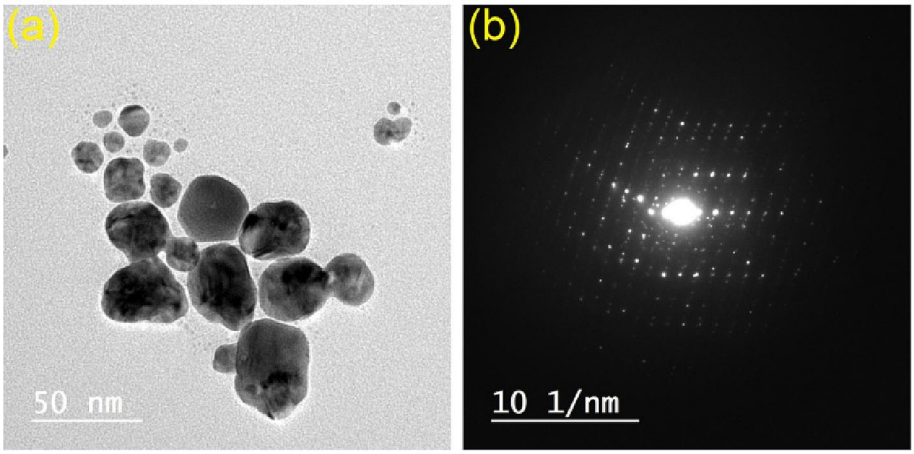

FIGURE 1 Transmission electron microscopy (TEM) images of mordant–anthocyanin complex nanoparticles.

The use of mordant–anthocyanin complex in the nano-scaled particle form is useful to better distribute the mordant–anthocyanin chromogenic active sites in the crosslinked resin matrix generated on the paper surface. Screen printing was used to apply the thermochromic nanocomposite onto cellulose paper sheets, and then the printed pattern was thermally fixed. The morphologies of the thermochromic prints were analyzed using SEM, as shown in Figure 2. The scanning electron micrographs show that the mordant–anthocyanin complex nanoparticles were successfully deposited on the paper surface. The microscopic SEM images also proved that the mordant–anthocyanin nanoparticles were uniformly dispersed across the paper surface by the screen-printing method. This uniform distribution of the mordant–anthocyanin nanoparticles can be explained by the creation of coordination bonds between the iron mordant, and the lone pairs of electrons on both the cellulose hydroxyl groups from one side and the anthocyanin hydroxyl groups from the other side. Fibrous morphological structures identical to blank paper were observed in the screen-printed sheets, with the ink particles instead being evenly dispersed throughout the fibrous paper surface. Using energy-dispersive X-ray spectroscopy (EDS) (Table 2), we can see that the deposited resin layer has a uniform distribution of the mordant–anthocyanin nanoparticles over the document surface. Both the cellulosic sheets and the binder are composed of carbon and oxygen, while the mordant–anthocyanin nanoparticles are composed of carbon and oxygen with trace amounts of iron.

As reported in Table 2, EDS conducted research to determine the elemental composition and dispersion uniformity of the mordant–anthocyanin complex nanoparticles onto paper surface. Using EDS spectra, the chemical compositions were validated at the three investigated sites to indicate relatively identical contents for the same sample, suggesting that the distribution of the mordant–anthocyanin nanoparticles on the printed sheets is homogeneous. The ratios employed in the preparation of the thermochromic inks matched those found in the EDS elemental analysis of the screen-printed films. FTIR spectroscopy has been an important analytical tool for identifying functional groups on a certain surface. FTIR spectroscopy can be used to determine how the thermochromic composite is attached to

TABLE 2 Chemical contents of INK_0, INK_1, and INK_8 at three separate spots on the sample surface.

Print		Carbon	Oxygen	Iron
INK_0		62.26	38.74	0
INK_1	Spot 1	62.58	37.57	0.85
	Spot 2	62.88	37.00	0.78
	Spot 3	62.71	37.41	0.88
INK_8	Spot 1	62.73	37.47	0.76
	Spot 2	62.35	37.82	0.83
	Spot 3	62.48	37.80	0.73

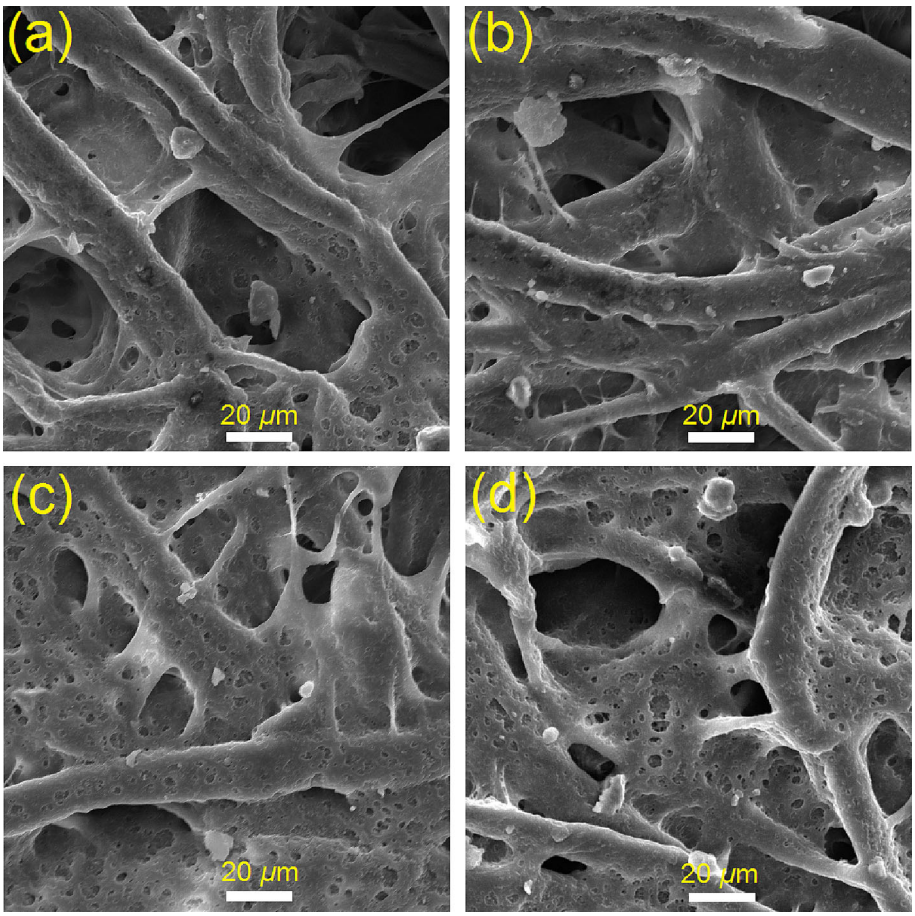

FIGURE 2 Scanning electron microscopy (SEM) micrographs of INK_1 (a, b), and INK_8 (c, d).

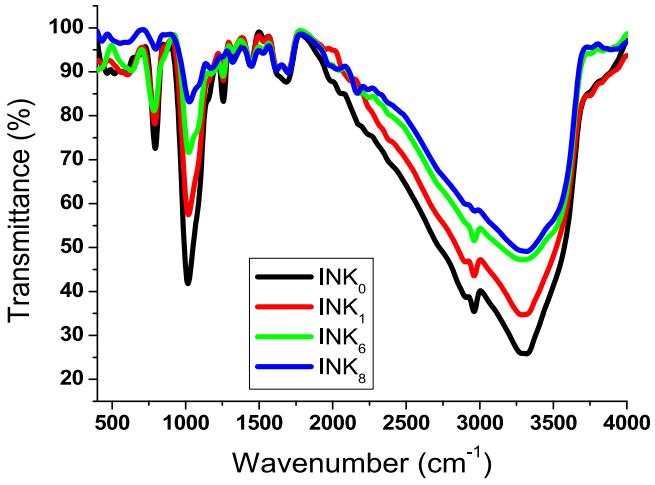

FIGURE 3 Fourier-transform infrared (FTIR) spectra of screen-printed samples: INK_0, INK_1, INK_6, and INK_8.

the cellulose sheet surface. The FTIR spectroscopic information for INK_0, INK_1, and INK_8 is shown in Figure 3. The existence of cellulose was verified by the strong absorbance intensity of the hydroxyl groups detected at 3312 cm^{-1}. The aliphatic C–H substituents in the glucose units were detected by their absorbance at 2958 cm^{-1}. After encapsulating the mordant–anthocyanin nanoparticles in the resin film, a strong binding is established between binder and cellulose. The absorption band by the resin carbonyl ester is measured at 1691 cm^{-1}. The anthocyanin-printed samples had a change in the position of the hydroxyl absorbance peak, which moved from 3312 cm^{-1} for INK_0 to 3299 cm^{-1} for the printed sheet from INK_1 to INK_8. The screen-printing technology also caused a decrease in the absorbance band caused by the resin carboxyl groups and cellulose hydroxyl groups [34], which can be explained by the formation of hydrogen bonds between the hydroxyl groups of the paper surface and the alkyd resin. A similar trend of diminishing hydroxyl group intensity was seen when the mordant–anthocyanin nanoparticles concentration was raised.

3.2 | Thermochromic measurements

A simple strategy was developed for the preparation and application of a print onto paper surface with the ability to switch color in response to temperature increase. Multiple concentrations of mordant–anthocyanin nanoparticles were utilized to create the thermochromic nanocomposite layer on the paper surface. The alkyd resin binder was used to entrap the mordant–anthocyanin nanoparticles onto the paper surface. The nanoparticles-containing alkyd binding agent crosslinks during thermofixation [35]. The printed samples exhibited thermochromism with high reversibility without fatigue. All printed samples had the same absorption wavelength detected at 418 nm. As the amount of the mordant–anthocyanin nanoparticles was raised, so was the strength of the absorption band. The layer printed on the paper sheet changed color from pink (25°C) to greenish-yellow (75°C) when exposed to heating. The color change is due to the thermochromic effect. For the naked eye, the temperature-induced greenish-yellow (75°C) color (λ_{max} = 552 nm) of the printed sample stood out against the paper's pink (25°C) background (λ_{max} = 418 nm), displaying an isosbestic point at 502 nm. All printed samples showed reversible thermochromic switching when exposed to a heating source at 25 and 75°C. It was found that increasing the temperature from 25 to 75°C caused a change in color from pink to greenish-yellow. This colorimetric change was reversible without fatigue over several cycles by cooling back to 25°C. By analyzing the colorimetric results, we were able to gauge the thermochromic activity of the anthocyanin-printed sheets. The findings of colorimetric experiments done using the CIELab parameters to detect the colorimetric shifts when exposed to various temperatures are shown in Table 3. All anthocyanin-printed paper sheets exhibited the same pink color. The blank paper sample (INK_0) displayed an off-white color. This indicates a translucence appearance of the thermochromic screen-printed film, designating a slight variation in the colorimetric measurements after printing showing the formation of a pale pink color for INK_1. This can be ascribed to the low ratio of the required mordant–anthocyanin nanoparticles dispersed through the homogenous nanocomposite matrix. Significant shifts in K/S and CIELab were monitored when the concentration of the mordant–anthocyanin complex nanoparticles was raised from INK_1 to INK_8, suggesting the production of a deeper pink hue. As the concentration of the mordant–anthocyanin nanoparticles increased from INK_1 to INK_8, significant shifts were monitored in K/S and CIELab upon increasing the temperature, suggesting the production of the paler greenish-yellow hue. The colorimetric alteration from pink to greenish-yellow was shown by an increase in L^* upon increasing the temperature. Upon exposure to higher temperatures, both $+a^*$ and $-b^*$ values shifted to $-a^*$ and $+b^*$ values, respectively. As the mordant–anthocyanin ratio increases, the intensity of the greenish-yellow absorption increases; however, once the concentration of the mordant–anthocyanin nanoparticles is greater than INK_6, the color strength remains constant. As compared to paper sheets with lower concentrations of mordant–anthocyanin nanoparticles (weaker greenish-yellow absorption band) (INK_1 to INK_5), and paper sheets with higher concentrations of mordant–anthocyanin nanoparticles (INK_7 and INK_8), the screen-printed INK_6 sample had the optimum thermochromic colorimetric properties.

Intramolecular charge transfer on the molecular structure of anthocyanin can be triggered by heat, leading to the formation of the corresponding highly extended molecular form [30–33]. Figure 4 shows the thermochromic properties of a paper sheet printed with the mordant–anthocyanin complex nanoparticles. Examining the CIELab parameters and absorbance spectra of the pink INK_6 was done to elucidate the thermochromism of the anthocyanin-printed sheet. Significant shifts in K/S and CIELab values were seen when the temperature was raised from 25 to 75°C, suggesting the production of a greenish-yellow hue (Figure 5). Using alternate heat and cold cycles, it was found that the anthocyanin-printed paper sheet was very resilient to thermal stress.

TABLE 3 Colorimetric screening of thermochromic prints with various ratios of mordant–anthocyanin nanoparticles at 25 and 75°C.

	K/S		*L**		*a**		*b**	
Prints	**25°C**	**75°C**	**25°C**	**75°C**	**25°C**	**75°C**	**25°C**	**75°C**
INK_0	0.23	0.19	91.25	91.61	0.08	0.11	1.51	1.45
INK_1	1.16	0.70	79.82	88.13	1.27	−12.70	−1.62	5.24
INK_2	1.28	0.81	79.40	86.57	1.66	−12.00	−1.70	6.43
INK_3	1.33	0.92	78.93	85.45	2.02	−10.31	−1.93	8.30
INK_4	1.61	1.07	77.84	83.96	2.46	−9.55	−2.15	10.50
INK_5	2.76	1.30	75.93	82.44	2.90	−8.86	−2.56	13.99
INK_6	2.82	1.45	75.47	80.06	3.72	−8.34	−2.81	17.03
INK_7	2.03	1.34	75.10	79.72	4.02	−6.70	−3.00	21.40
INK_8	2.17	1.52	74.91	78.85	4.09	−6.01	−3.14	21.78

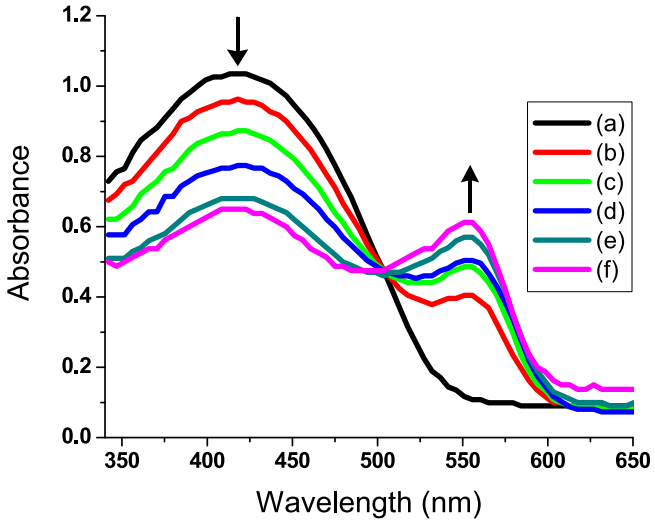

FIGURE 4 Ultraviolet-visible (UV-vis) absorbance spectra of INK_6 at 25°C (a), 35°C (b), 45°C (c), 55°C (d), 65°C (e), and 75°C (f).

To test the fatigue resistance of the thermochromic prints, we subjected it to repeated heating (75°C) and cooling (25°C) conditions for a set number of cycles. Several cycles of colorimetric changes were completed without any signs of fatigue (Figure 6). With their interesting thermochromic property, the printed sheets are well-suited for use in anti-counterfeiting purposes.

The hydroxyl functional groups on both cellulose and anthocyanidin form a coordinated mordant–anthocyanidin complex [31–33]. The level of coordination was found to decrease when the temperature increases. Therefore, a number of distinctive colorimetric shades were observed with increasing the temperature as shown in Figure 7.

3.3 | Rheological and mechanical studies

As reported in Figure 8, the rheological flow profile of INK_6 fluid was explored. The composite ink was not viscous because its flow profile was observed to conform to Newton's equations. The viscosity was found to drop down linearly when the shear stress was increased. The relationship between viscosity and shear rate was monitored to be linear. It was observed that the fluid viscosity quickly decreased, nearing equilibrium, both at high and low shear rates.

In order to examine the mechanical performance, the produced nanocomposite ink was used to completely cover the sheet sample. The prints on the paper sample resulted in slightly greater tensile strength than blank Whatman sheets (INK_0), despite the absence of the mordant–anthocyanin nanoparticles. Thus, the anthocyanin-free composite fluid was found to be responsible for the observed strain percent. The anthocyanin-free composite fluid was mostly composed of an organic-based alkyd resin binder. The percentage of strain in INK_0 was slightly higher than in INK_1. The Young's modulus of INK_0 was shown to decrease at or around the strain percent. This could be due to the tensile/strain dependency of Young's modulus [36]. The flexibility and adherence of INK_0 were shown by the alkyd binder, a critical component of the nanocomposite ink that was applied onto the paper surface. The increased concentrations of mordant–anthocyanin nanoparticles were shown to alter the mechanical performance of the printed sheets (Figure 9). An increase in the mordant–anthocyanin concentration from INK_1 to INK_6 resulted in a rise in Young's modulus and tensile strength. Although the ratio of the mordant–anthocyanin nanoparticles in the coated samples increased from INK_6 to INK_8, the value remained almost the same. Minor shifts in strain percent at break were seen once the mordant–anthocyanin concentration rose from INK_1 to INK_8. Interfacial crosslinks between the positively charged mordant–anthocyanin complex and the negative charges created on the cellulose surface by treating with aqueous NH_4OH to slightly deprotonate the cellulose hydroxyl groups. Coordination binding of the positively charged mordant–anthocyanin complex with the negative charges on the cellulose enhanced the crosslinking between cellulose fibers when the mordant–anthocyanin complex was immobilized on the paper surface. Up to INK_6, the tensile strength rose proportionally with increasing the total concentration of the mordant–anthocyanin complex nanoparticles. Due to the coagulation of the mordant–anthocyanin nanoparticles, which caused the expansion of the inter-fiber gaps, there was no difference in tensile strength between INK_6, INK_7 and INK_8. Using screen-printing

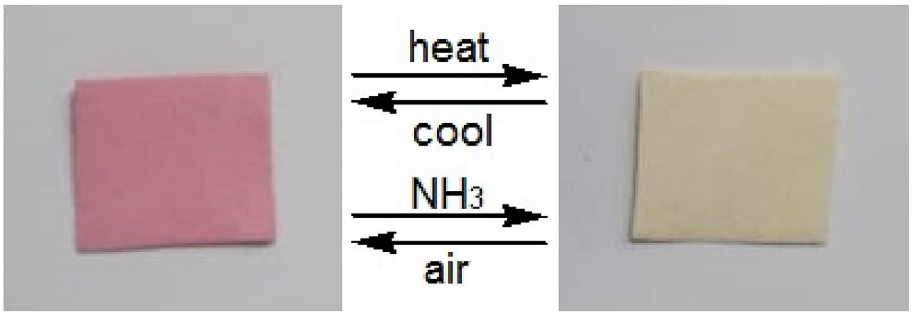

FIGURE 5 Thermochromism of INK_6 demonstrating a change in color from pink to greenish-yellow upon heating from 25 to 75°C, respectively. The same behavior was detected demonstrating a reversible color change under air and ammonia gas conditions.

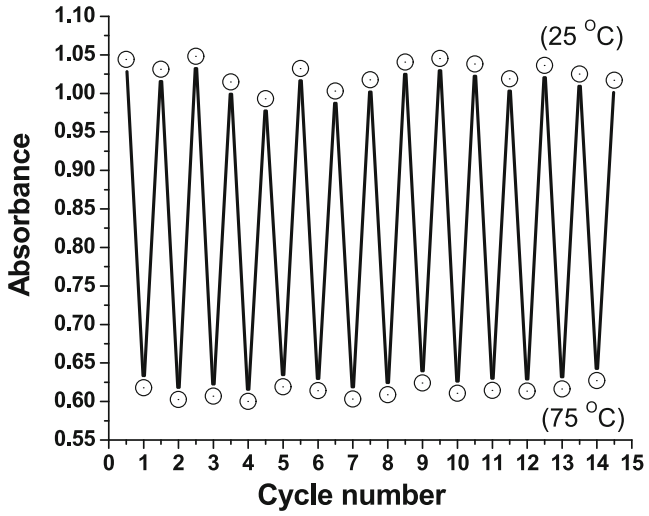

FIGURE 6 Fatigue resistance to reversibility of the absorption intensity at 552 nm (INK_6) under repeated heating (75°C) and cooling (25°C) conditions for several cycles.

technology, the nanocomposite inks were included onto paper sheets, creating anti-counterfeiting prints with the smoothest surface conceivable without sacrificing the document pliability.

3.4 | Vapochromic measurements

It has been crucial to design sensor materials capable of detecting gaseous and aqueous ammonia [37–40]. The microfibrous cellulose has a large surface area, making it ideal for absorbing and diffusing analytes like ammonia quickly across the mesh, resulting in excellent sensitivity [41–46]. INK_6 displayed a rapid color change from pink (λ_{max} = 418 nm) to greenish-yellow (λ_{max} = 552 nm) upon exposure to ammonia gas, correlating to the emergence of a prominent absorbance peak in the absorption spectra at 552 nm as illustrated in Figure 10. An isosbestic point was detected at 502 nm. A fast reversal to pink occurs when the printed test strip is shielded from the ammonia source. Once the paper strip has been exposed to ammonia again, it will regenerate the greenish-yellow color. Figure 11 shows a color

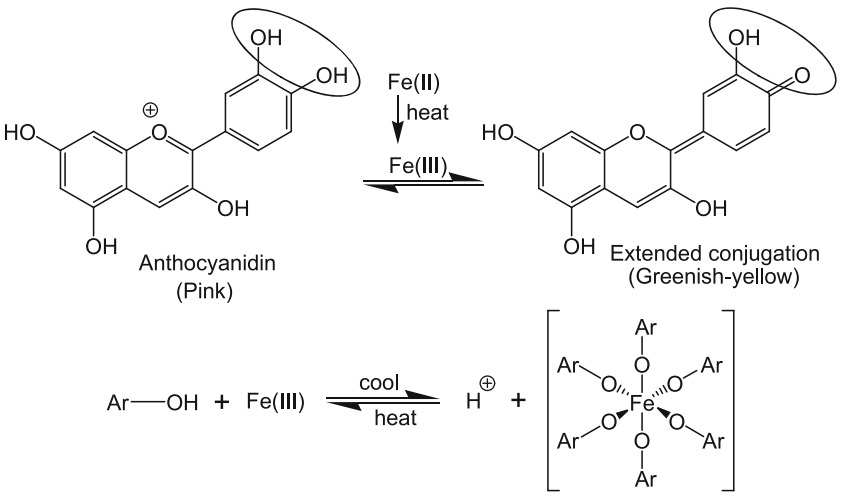

FIGURE 7 Suggested thermochromic mechanism for the formation–dissociation reversible process of a mordant–anthocyanidin complex; Ar is anthocyanidin comprising hydroxyl groups.

change of INK_6 from dark pink to light pink, dark green, light green, and greenish-yellow upon increasing ammonia concentration in aqueous medium from 0 to 50, 100, 200 and 300 ppm, respectively. The test dipstick reversibility to ammonia gas was determined by reporting the absorbance at 552 nm after 1–5 s of exposure to ammonia gas over several cycles. Based on the findings, the reversible colorimetric switching was shown to be fatigue-free across several cycles. There are several possible uses for the existing simple and effective ammonia sensor, including monitoring human health, protecting the environment, and improving manufacturing processes.

The detection limit for aqueous ammonia was investigated by submerging the anthocyanin-printed paper strip in solutions of varying ammonia concentrations for 1–5 s. After the paper had air-dried, the variations in absorption wavelength were reported. When the quantity of aqueous ammonia is raised from 50 to 300 ppm, we can see that the absorbance wavelength changes from 418 to 552 nm, indicating a bathochromic shift as illustrated in Figure 12. At 50 ppm of aqueous ammonia, an absorption band appeared at 552 nm. The absorption at 552 nm rises linearly with increasing aqueous ammonia content. When the ammonia concentration was increased to above 300 ppm; however, no increment was monitored in the absorbance intensity. Thus, 50–300 ppm is given as the detection range for aqueous ammonia.

There is a theory that gaseous ammonia serves as a Brønsted base (proton acceptor), whereas anthocyanin biomolecule functions as a Brønsted acid (proton donor) [26–31]. This results in deprotonation of anthocyanidin chromophore to allow electrons to flow on the anthocyanin molecular system. This creates an extended conjugate

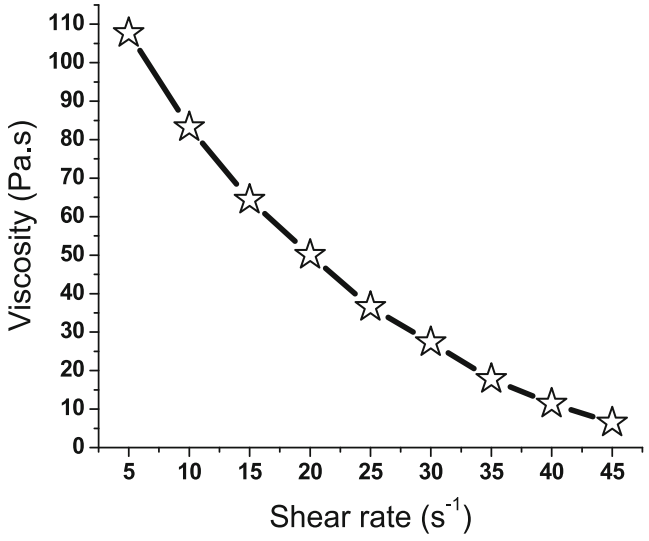

FIGURE 8 Viscosity of INK_6 ink versus shearing rate.

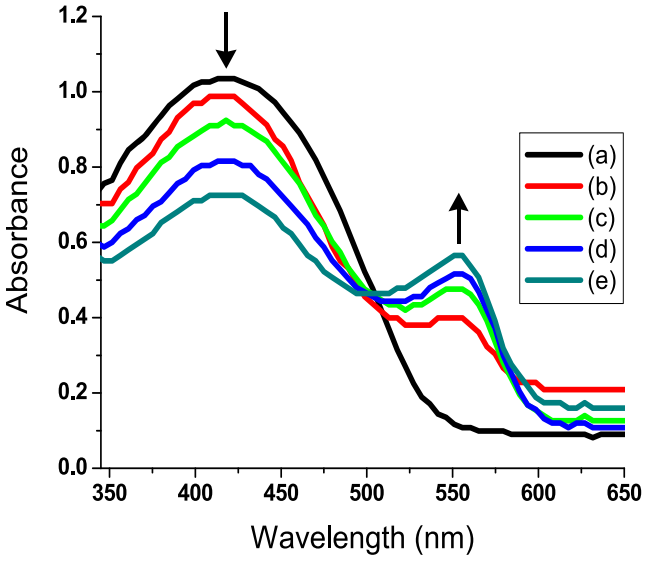

FIGURE 10 Absorption spectra of INK_6 under air and ammonia gas conditions: 0 ppm (a), 50 ppm (b), 100 ppm (c), 200 ppm (d), and 300 ppm (e).

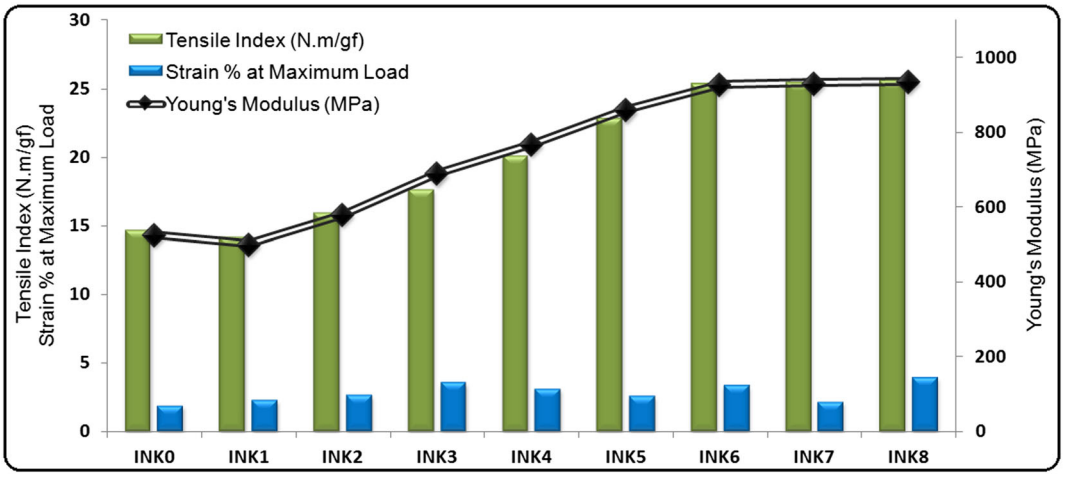

FIGURE 9 Effect of mordant–anthocyanin complex nanoparticles content on the mechanical performance of printed documents.

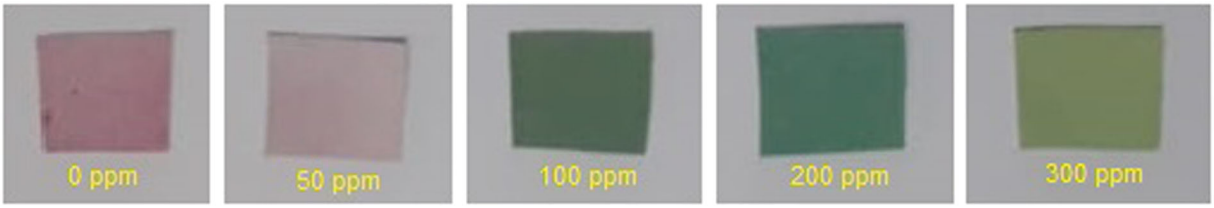

FIGURE 11 Color change of INK_6 from dark pink (0 ppm) to light pink (50 ppm), dark green (100 ppm), light green (200 ppm), and greenish-yellow (300 ppm) upon increasing ammonia gas.

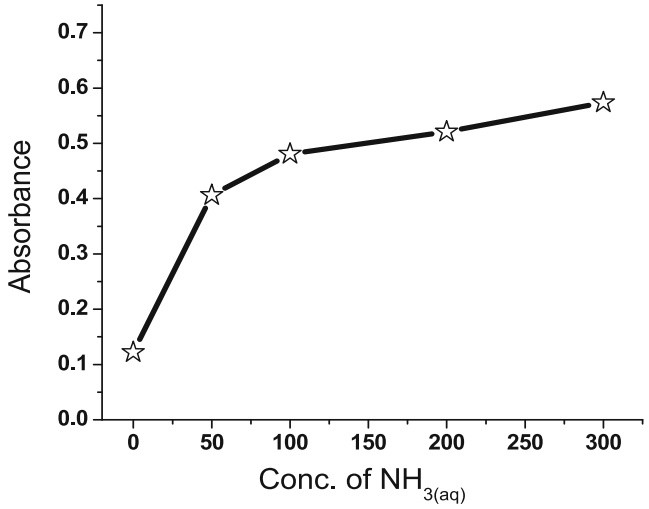

FIGURE 12 Absorption intensity of INK_6 as a function of aqueous ammonia concentration.

TABLE 4 CIELab coordinates of INK_6 in the presence of amine vapors released by boiling.

Amine (vapor)	L^*	a^*	b^*
Ammonia	86.05	−9.54	18.95
Ethylamine	77.32	−2.63	8.60
n-Butylamine	78.21	−2.84	8.93
Piperidine	80.60	−2.70	11.75
Diethylamine	79.05	−2.62	10.40
Triethylamine	77.79	−2.87	8.72
Tributylamine	76.13	−2.56	8.32
Aniline	75.37	4.33	−2.87
Pyridine	75.70	3.82	−2.63

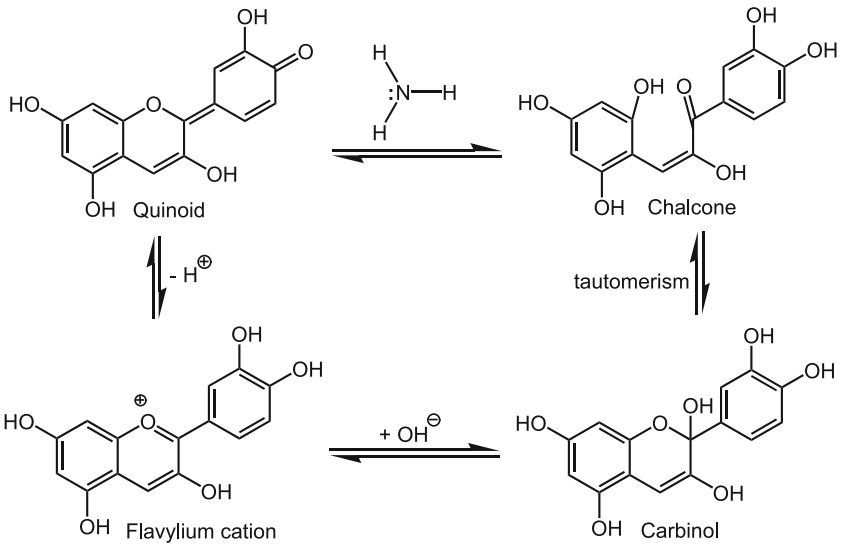

SCHEME 1 Proposed vapochromic mechanism for detection of ammonia by anthocyanidin.

molecular system, which triggers the colorimetric change (Scheme 1). Thus, the printed paper sheet (INK_6) can be used for visual detection of ammonia vapor and aqueous phases.

In order to explore the sensor selectivity, INK_6 was exposed to various amines and organic solvents. The aromatic amines were undetectable as shown in Table 4. The sensor selectivity was found to depend on the relative basicity of various amines in the order of secondary > primary > tertiary amines. CIELab coordinates were unchangeable upon the exposure of INK_6 to the fumes of various solvents, including dichloromethane, acetic acid, cyclohexane, methanol, ethanol, acetone, formic acid, toluene, chloroform, water, dimethyl sulfoxide, and benzene. Thus, it can be concluded that there is no evidence of interference between INK_6 and the detection of ammonia in the presence of those solvents.

4 | CONCLUSION

In conclusion, after being exposed to gaseous ammonia for a second, and heat at 75°C, the multi-stimuli responsive paper sheets showed vapochromic and thermochromic activities, respectively. Anthocyanidin chromic agent was extracted from red-cabbage, and used as active detection sites for the preparation of composite ink using ferrous sulfate as mordant. The anthocyanidin-printed sheets displayed fatigue resistance to reversibility. Color changes were monitored from pink to greenish-yellow upon exposure to ammonia or heat. Paper strips printed with mordant–anthocyanin complex nanoparticles were submerged in aqueous solutions of varying concentrations of ammonia to show a detection range of 50–300 ppm. The papers were printed with a composite ink that included mordant–anthocyanin complex nanoparticles. The mechanical and physical characteristics of the printed papers were not altered by the addition of mordant–anthocyanin complex nanoparticles; however, they were found to be useful in the construction of authenticating nanocomposite films used in anti-counterfeiting applications. An alkyd binder was used as a bulk to attach the mordant–anthocyanin complex nanoparticles onto the paper surface. This approach can be utilized to produce a simple and low-cost authentication print with great durability without compromising the mechanical qualities of the printed sheet. Two absorption peaks, 418 and 552 nm, were detected in the screen-printed paper sheets. TEM analysis of dispersed mordant–anthocyanin nanoparticles showed spherical morphology with diameters between 4 and 19 nm. SEM, FTIR, EDS, CIELab, and absorbance spectra were all used to analyze the printed paper sheets. Off-white papers were screen-printed with pink ink, and became greenish-yellow when exposed to heat or ammonia. The rheology of the nanocomposite ink was investigated. The current nanocomposite films were developed for a range of potential products, including anti-counterfeiting and sensing purposes.

ACKNOWLEDGMENTS

Princess Nourah bint Abdulrahman University Researchers Supporting Project number (PNURSP2023R22), Princess Nourah bint Abdulrahman University, Riyadh, Saudi Arabia.

CONFLICT OF INTEREST STATEMENT

The authors declare that they have no known competing financial interests or personal relationships that could have appeared to influence the work reported in this article.

DATA AVAILABILITY STATEMENT

All relevant data are within the manuscript and available from the corresponding author upon request.

ORCID

Nashwa M. El-Metwaly https://orcid.org/0000-0002-0619-6206

REFERENCES

[1] A. Hazra, U. Mondal, S. Mandal, P. Banerjee, *Dalton Trans.* **2021**, *50*, 8657.
[2] X. Yu, H. Zhang, J. Yu, *Aggregate* **2021**, *2*, 20.
[3] H. Liang, Y. Liu, F. Zhou, C. Zhang, L. Yang, L. Zhao, Y. Li, Y. Xu, T. Wang, X. Hua, Y. Zhu, H. Li, *Chem. Sci.* **2022**, *13*, 14191.
[4] A. A. Ansari, K. M. Aldajani, A. N. AlHazaa, H. A. Albrithen, *Coord. Chem. Rev.* **2022**, *462*, 214523.
[5] H. Suo, Q. Zhu, X. Zhang, B. Chen, J. Chen, F. Wang, *Mater. Today Phys.* **2021**, *21*, 100520.
[6] G. Huang, Q. Xia, W. Huang, J. Tian, Z. He, B. Shi Li, B. Z. Tang, *Angew. Chem.* **2019**, *131*, 17978.
[7] S. D. Al-Qahtani, A. Hameed, R. M. Snari, R. Shah, A. A. Alfi, N. M. El-Metwaly, *J. Mol. Liq.* **2022**, *354*, 118927.
[8] W. Hong, Z. Yuan, X. Chen, *Small* **2020**, *16*, 1907626.
[9] K. Muthamma, D. Sunil, P. Shetty, *Appl. Mater. Today* **2021**, *23*, 101050.
[10] Y. Chen, J. Lin, J. Fu, R. Ye, L. Lei, Y. Shen, D. Deng, S. Xu, *J. Lumin.* **2022**, *252*, 119404.
[11] Z. Li, X. Liu, G. Wang, B. Li, H. Chen, H. Li, Y. Zhao, *Nat. Commun.* **2021**, *12*, 1.
[12] H. Zhang, D. Hua, C. Huang, S. K. Samal, R. Xiong, F. Sauvage, K. Braeckmans, K. Remaut, S. C. De Smedt, *Adv. Mater.* **2020**, *32*, 1905486.
[13] Z. Wang, H. Yuan, Y. Zhang, D. Wang, J. Ju, Y. Tan, *J. Mater. Sci. Technol.* **2022**, *101*, 264.
[14] M. Ni, W. Luo, D. Wang, Y. Zhang, H. Peng, X. Zhou, X. Xie, *ACS Appl. Mater. Interfaces* **2021**, *13*, 19159.
[15] H. Alidaei-Sharif, H. Roghani-Mamaqani, M. Babazadeh-Mamaqani, K. Sahandi-Zangabad, A. Abdollahi, M. Salami-Kalajahi, *J. Photochem. Photobiol. A Chem.* **2023**, *436*, 114343.
[16] Z. Li, G. Wang, Y. Ye, B. Li, H. Li, B. Chen, *Angew. Chem.* **2019**, *131*, 18193.
[17] T. Wei, B. Jia, L. Shen, C. Zhao, L. Wu, B. Zhang, X. Tao, S. Wu, Y. Liang, *J. Eur. Ceram. Soc.* **2020**, *40*, 4153.
[18] P. H. N. Crosby, A. N. Netravali, *Adv. Sustain. Syst.* **2022**, *6*, 2200208.
[19] J. Lin, P. Wang, H. Wang, Y. Shi, K. Zhu, F. Yan, G. Li, H. Ye, J. Zhai, X. Wu, *Adv. Opt. Mater.* **2021**, *9*, 2100580.
[20] Y. Wu, R. Sun, J. Ren, S. Zhang, S. Wu, *Adv. Funct. Mater.* **2022**, *33*, 2210047.
[21] L. Zhang, H. Xia, F. Xia, Y. Du, Y. Wu, Y. Gao, *ACS Appl. Energy Mater.* **2021**, *4*, 9783.
[22] M. W. Khalid, C. Whitehouse, R. Ahmed, M. U. Hassan, H. Butt, *Adv. Opt. Mater.* **2019**, *7*, 1801013.
[23] M. H. El-Newehy, H. El-Hamshary, W. M. Salem, *Polymer* **2021**, *13*, 531.
[24] N. Boens, B. Verbelen, M. J. Ortiz, L. Jiao, W. Dehaen, *Coord. Chem. Rev.* **2019**, *399*, 213024.
[25] S. D. Al-Qahtani, O. A. Azher, R. Felaly, A. Subaihi, J. Alkabli, O. Alaysuy, N. M. El-Metwaly, *Int. J. Biol. Macromol.* **2021**, *182*, 2037.
[26] M. E. El-Naggar, M. H. El-Newehy, A. Aldalbahi, W. M. Salem, T. A. Khattab, *J. Environ. Chem. Eng.* **2021**, *9*, 105072.
[27] M. Alsahag, A. Alisaac, G. A. A. Al-Hazmi, R. A. Pashameah, R. M. S. Attar, F. A. Saad, N. M. El-Metwaly, *Int. J. Biol. Macromol.* **2023**, *224*, 233.
[28] B. Kuswandi, N. P. N. Asih, D. K. Pratoko, N. Kristiningrum, M. Moradi, *Packag. Technol. Sci.* **2020**, *33*, 321.
[29] A. Alisaac, M. Alsahag, M. Alshareef, R. M. Snari, M. Alhasani, H. M. Abumelha, N. M. El-Metwaly, *Inorg. Chem. Commun.* **2022**, *145*, 110023.
[30] A. Pakolpakçıl, B. Osman, G. Göktalay, E. T. Özer, Y. Şahan, B. Becerir, E. Karaca, *J. Polym. Res.* **2021**, *28*, 1.
[31] S. D. Al-Qahtani, H. K. Alzahrani, O. A. Azher, Z. O. Owidah, M. Abualnaja, T. M. Habeebullah, N. M. El-Metwaly, *J. Environ. Chem. Eng.* **2021**, *9*, 105493.
[32] X. Zhai, Y. Sun, S. Cen, X. Wang, J. Zhang, Z. Yang, Y. Li, X. Wang, C. Zhou, M. Arslan, Z. Li, *Food Hydrocoll.* **2022**, *133*, 107989.

[33] A. Nafady, A. M. Al-Enizi, A. A. Alothman, S. F. Shaikh, *Talanta* **2021**, *230*, 122292.
[34] O. M. Mokhtar, Y. A. Attia, A. R. Wassel, T. A. Khattab, *Luminescence* **1933**, *2021*, 36.
[35] S. F. Ibarhiam, H. F. Alshareef, S. A. Alqarni, R. Shah, S. D. Al-Qahtani, S. J. Almehmadi, N. M. El-Metwaly, *React. Funct. Polym.* **2022**, *172*, 105186.
[36] M. M. Abdelhameed, Y. A. Attia, M. S. Abdelrahman, T. A. Khattab, *Luminescence* **2021**, *36*, 865.
[37] D. Zhang, S. Yu, X. Wang, J. Huang, W. Pan, J. Zhang, B. E. Meteku, J. Zeng, *J. Hazard. Mater.* **2022**, *423*, 127160.
[38] D. Zhang, Z. Kang, X. Liu, J. Guo, Y. Yang, *Sens. Actuators B Chem.* **2022**, *357*, 131419.
[39] D. Zhang, Y. Luo, Z. Huang, M. Tang, J. Sun, X. Wang, X. Wang, Y. Wang, W. Wu, F. Dai, *J. Colloid Interface Sci.* **2023**, *630*, 776.
[40] D. Wang, D. Zhang, Y. Yang, Q. Mi, J. Zhang, L. Yu, *ACS Nano* **2021**, *15*, 2911.
[41] K. Ratajczak, M. Stobiecka, *Carbohydr. Polym.* **2020**, *229*, 115463.
[42] S. Abdelmoez, R. A. Abd El Azeem, A. A. Nada, T. A. Khattab, *Z. Anorg. Allg. Chem.* **2016**, *642*, 219.
[43] A. M. Binyaseen, A. Bayazeed, S. Y. Al-nami, K. Abu Al-Ola, S. A. Alqarni, S. H. Abdel-Hafez, N. M. El-Metwaly, *Ceram. Int.* **2022**, *48*, 4841.
[44] T. A. Khattab, M. S. Abdelrahman, *Advances in Functional Finishing of Textiles*, Vol. 257, Matthew Deans, India **2020**.
[45] R. B. Alnoman, S. D. Al-Qahtani, A. Bayazeed, A. M. Munshi, A. Alsoliemy, S. A. Alqarni, N. M. El-Metwaly, *ACS Omega* **2022**, *7*, 5595.
[46] A. G. Hassabo, A. L. Mohamed, T. A. Khattab, *Luminescence* **2022**, *37*, 21.

How to cite this article: A. M. Aldawsari, N. D. Alkhathami, A. M. Al-bonayan, H. Alessa, K. M. Alkhamis, H. M. Abumelha, N. M. El-Metwaly, *Luminescence* **2023**, *38*(5), 613. https://doi.org/10.1002/bio.4487